T5 Ion Engine Plume Analysis using a Time of Flight Mass Spectrometer.

by

David H Mundy
Space Department,
Defence Evaluation and Research Agency,
Farnborough,
Hampshire,
GU14 0LX,
UK

Abstract

The work reported on here used the Aerospace Corporation's time of flight mass spectrometer to investigate the relative intensities of Xe^{+}, Xe^{+2}, Xe^{+3} and Fe^{+} seen in the exhaust plume of a T5 ion engine. The data recorded at each operating point investigated were used to generate thrust correction factors and to estimate the rate of loss of iron from the discharge chamber. From these data relationships between thrust correction factor and both anode voltage and anode current were developed, along with discharge chamber erosion rates and estimated lifetimes. Further examination of the data indicates that, for a given thrust level, thrust correction factor and iron loss rate are best correlated with mass utilisation efficiency rather than anode voltage, anode current or main flowrate.

Introduction

Ideally, all the high velocity particles emerging from an ion engine would be singly-charged xenon ions. However, a small proportion of the high velocity ions will be doubly and triply-charged xenon ions as well as there being traces of metallic ions.

The presence of doubly and triply-charged xenon ions reduces the thrust that would otherwise be expected from measuring the beam accelerating potential and the beam ion current. The effects of doubly and triply-charged ions on the thrust are represented by a correction coefficient α_{ion}.

The flux density of metallic ions is so low that there is no discernible effect on the thrust. These ions are primarily sourced from the discharge chamber and screen grid. If the flux density of these metallic ions can be determined then it should be possible to calculate the mass erosion rate from the discharge chamber at a variety of operating points. These erosion rates can then be converted to discharge chamber lifetime estimations.

© British Crown copyright 1997 DERA. Published by the Electric Rocket Propulsion Society, with permission.

The investigation reported in this paper used Aerospace Corporation's well proven time of flight mass spectrometer (TOFMS)[1] mounted on a rotation table to measure the relative intensities in the ion beam of Xe^{+}, Xe^{+2}, Xe^{+3} and Fe^{+} at a variety of operating conditions. Although Mo^{+2} was detected, no data on this particular ion will be presented in this paper. Calculation of discharge chamber erosion rates and hence lifetimes assumed that the ion beam is azimuthally symmetric; this has been demonstrated by earlier work carried out in the UK[2].

Method

The ion thruster used in this work was an engineering model T5 MkIV[3], fitted with a flight standard 'optimised' grid-set as shown in Fig.1. It was mounted

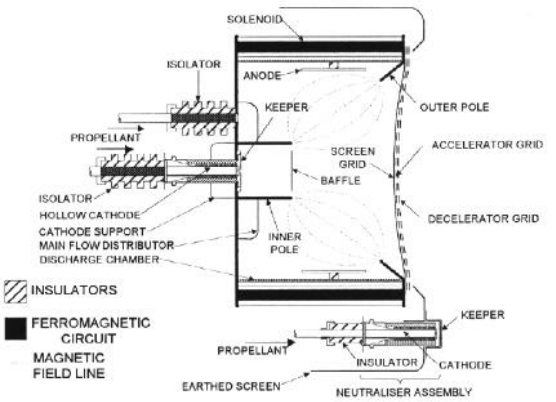

Fig.1 Schematic Diagram of the T5 MkIV ion thruster

in a large cryogenically pumped test facility at the Aerospace Corporation. This facility is capable of maintaining a background pressure of $2x10^{-6}$ torr,corrected for xenon, at the flowrates investigated.

The parallel plate deflector of the TOFMS[1] (see Fig.2) acts as a medium resolution energy filter ($\Delta E \approx 8eV$) that rejects low velocity ions and enhances the signal to background ratio of the time of flight spectra. The parallel plate deflector voltage (V_{rep}) is set to pass ions that have been accelerated by the beam potential (1175V). For ions of a given energy, the mass of the ion or its charge have no effect on whether it can pass through the parallel plate deflector.

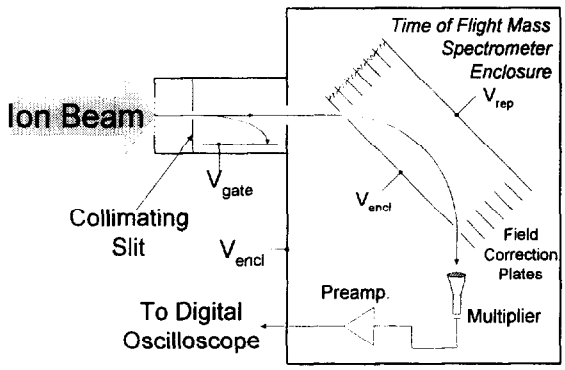

Fig.2 Functional Diagram of the Time of Flight Mass Spectrometer

The modulator voltage (V_{gate}) is normally set to deflect all the ions passing through the collimating slit so they do not pass into the parallel plate deflector. To sample the ion species in the thruster plume, the modulator voltage is pulsed off for a fixed duration, allowing a sample of ions into the device. These ions drift into the parallel plate deflector, only reaching the electron multiplier if they were accelerated by the beam voltage. The electron multiplier signal is fed into a pre-amplifier enclosed within the equipment giving a total gain of 45mV/μA. This signal is then fed via coaxial cable to a filter amplifier and a digital storage scope.

It can be shown that the time taken for an ion to travel from the collimating slit to the electron multiplier is proportional to the square root of the mass/charge ratio of the ion i.e. heavy single charged ions take longer to reach the electron multiplier than lighter multi-charged ions. This discrimination, at least in principle, allows the experimenter to differentiate between the five ion species mentioned above. The resultant scope trace

Parameter Name	Nominal Value
Beam Current (I_B)	318mA
Beam Voltage (V_B)	1175V
Anode Current (I_A)	2.00A
Anode Voltage (V_A)	42V
Magnet Current (I_{MAG})	170mA
Magnet Voltage (V_{MAG})	12V
Cathode Keeper Current(I_{CK})	1.00A
Cathode Keeper Voltage (V_{CK})	12V
Neutraliser Keeper Current (I_{NK})	660mA
Neutraliser Keeper Voltage (V_{NK})	22V
Accel. Grid Current (I_{ACC})	1.35mA
Accel. Grid Voltage (V_{ACC})	-250V
Decel. Grid Current (I_{DEC})	0.75mA
Decel. Grid Voltage (V_{DEC})	-50V
Main Flowrate ($\dot{m}_f$)	0.424mg/s
Cathode Flowrate ($\dot{m}_c$)	0.090mg/s
Neutraliser Flowrate ($\dot{m}_n$)	0.040mg/s
Thrust	18mN
Specific Impulse	3300s
Propellant Mass Utilisation Efficiency (η_m)	84%

Table 1
Nominal uncorrected 18mN operating point for ARTEMIS

shows a signal with a number of peaks, the heights of which reflect the relative numbers of different ion species in the beam. Note that as far as the mass spectrometer is concerned, a doubly charged ion of mass 56 is the same as a singly charged ion of mass 28.

The first of 15 thruster operating points under examination was set up. This was then used to set up the TOFMS and the rotary and linear actuators used to move the mass spectrometer around. It was decided that the thruster plume should be investigated at four angular positions to the ion thruster axis: 2^0, 6^0, 10^0, and 14^0.

Of the 15 operating points under examination, nine were at a fixed anode current of 2.07A with the following anode voltages, 42.2, 41.2, 39.6, 38.8, 37.5, 36.3, 40.2, 43.2, and 44.3V, set by varying the magnetic field. The peculiar order in which the anode voltages is listed reflects the order in which the voltages were examined, starting with the nominal 18mN operating point. The remaining six operating points were based around a fixed anode voltage of

41.0V with the following anode currents, 2.82, 2.60, 2.39, 2.20, 2.05, and 1.90A; the anode voltage was kept at 41.0V by varying the magnetic field current. Table 1 shows the value of the operational parameters required for 18mN operation around which the 15 operating points under examination were based.

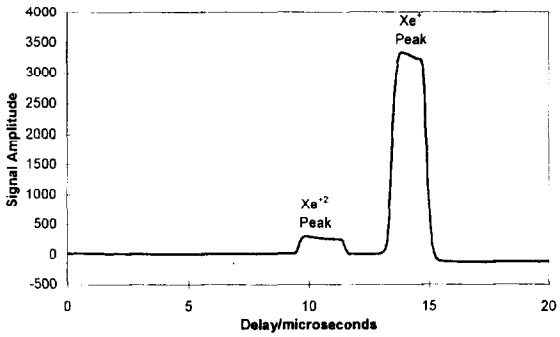

Fig.3 Typical Low Resolution TOFMS Data Set

In essence, this experiment was split into two parts. The first was to determine the relative intensities of Xe^{+}, Xe^{+2}, and Xe^{+3}. The second part of the experiment was to determine the relative intensity of Fe^{+} in the plume with respect to the xenon ion species.

The resultant raw data files require subjective judgement to determine relative intensity values, especially as the lowest values are sometimes virtually indistinguishable from background noise. This has little effect on the determination of α_{ion} as the Xe^{+2} signals are large and the contribution from Xe^{+3} is negligible (although still included). However, the relative intensities of Fe^{+} and Mo^{+2}, particularly at the high angles and low anode voltages, have significant errors associated with them. Fig.3 shows a typical data

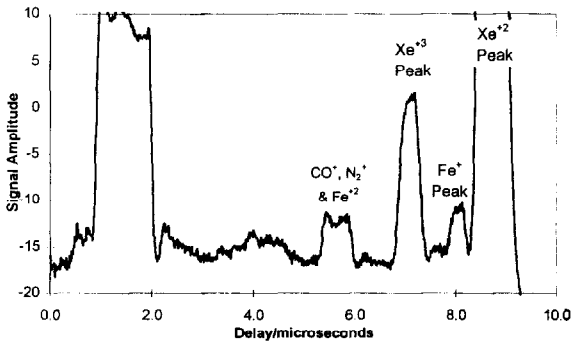

Fig.4 Typical High Resolution TOFMS Data Set

set from which the ratio of doubly to singly charged xenon can be determined; while Fig.4 shows a high resolution data set from which the relative intensity of Fe^{+} can be determined. The time of flight gate width for the high resolution data was set to attenuate the Xe^{+} signal but maintained the Xe^{+2} and lower mass/charge ratio ions at the same intensity as observed in the equivalent low resolution data set.

Results

Angular Position (deg)	Relative Mass Spectral Intensities			Angular α_{ion}	Composite α_{ion}
	Xe^{+}	Xe^{+2}	Xe^{+3}		
2	91.7%	8.2%	0.055	97.6%	
6	94.5%	5.4%	0.049	98.4%	
10	94.5%	5.5%	0.055	98.4%	**98.2%**
14	93.9%	6.0%	0.036	98.2%	

Table 2
Sample Mass Spectral Intensity Data

Consider Table 2 below, which shows the relative intensities of Xe^{+}, Xe^{+2}, and Xe^{+3} for a typical operating point at all four angular positions.

Columns two to four of Table 2 record the relative mass spectral intensities at each angle under investigation. This is simply calculated by dividing the relevant ion intensity by the sum of all three ion intensities. The equation used for calculating α_{ion} at each angular position is as follows:

$$\alpha_{ion} = \frac{Xe^{+}I + \frac{Xe^{+2}I}{\sqrt{2}} + \frac{Xe^{+3}I}{\sqrt{3}}}{Xe^{+}I + Xe^{+2}I + Xe^{+3}I} \qquad (1)$$

where: $Xe^{+}I$ Relative intensity of Xe^{+}.
$Xe^{+2}I$ Relative intensity of Xe^{+2}.
$Xe^{+3}I$ Relative intensity of Xe^{+3}.

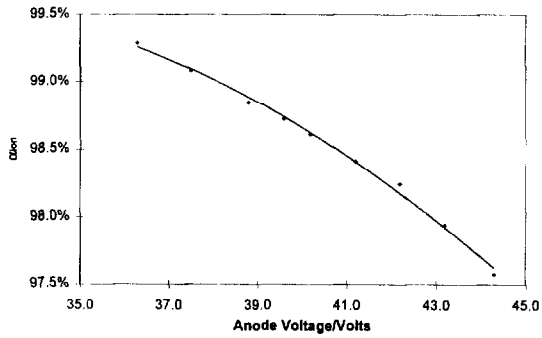

Fig.5 α_{ion} vs V_A for Constant Anode Current (2.07A) and Discharge Chamber Flowrate (0.524mg/s)

The four values of α_{ion} were averaged to give a composite value using two weighting factors. The first weighting factor was the absolute intensity of the Xe^{+} signal at each angular position and the second a term based on the elementary annular area over which the value of α_{ion} is valid.

For any given operating point the values calculated for α_{ion}, according to equation (1), varied slightly at each angular position as can be seen in Table 2 above.

Fig.5 shows how the value for α_{ion} changes with anode voltage while the anode current and xenon flowrates are kept constant. As expected, the presence of doubly-charged ions increases with an increased anode voltage. Fig.6 shows a similar relationship between α_{ion} and anode current for a fixed anode voltage and constant flowrates. Detailed explanations for both of these relationships is given later in this paper.

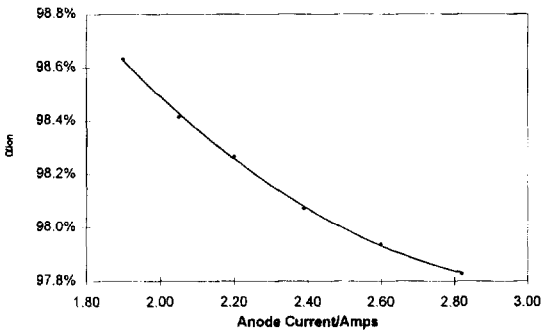

Fig.6 α_{ion} vs I_A for Constant Anode Voltage (41V) and Discharge Chamber Flowrate (0.524mg/s)

It is possible to convert the measured mass spectral intensities (or the relative mass spectral intensities) of the xenon ion species into fractional number densities using the following equation:

$$N^{+p} = \frac{(Xe^{+p}I)p^{-3/2}}{\sum_{n=1}^{3}(Xe^{+n}I)n^{-3/2}} \qquad (2)$$

where: N^{+p} Fractional number density of Xe^{+p} ions.

$Xe^{+p}I$ Relative mass spectral intensity of Xe^{+p}.

Fig.7 shows how the fractional number density of Xe^{+} and Xe^{+2} change with increasing anode voltage for a fixed anode current of 2.07A and discharge chamber flowrate of 0.524mg/s. The maximum contribution from Xe^{+3} (at 44.3V) was only 0.025%, so was not plotted. In fact, the effects of triply-charged xenon on α_{ion} are equally inconsequential. Note that mass utilisation efficiency is plotted on the x-axis rather than anode voltage to aid in comparison with Fig.8.

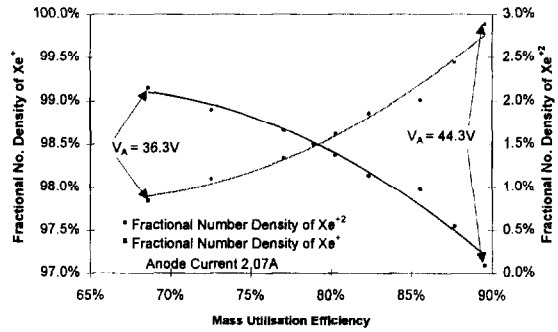

Fig.7 Fractional Number Densities of Xe^{+} and Xe^{+2} vs Anode Voltage

Fig.8 shows the effects of varying the anode current on the fractional number densities of Xe^{+} and Xe^{+2}. At first this seemed like a surprising result, as indeed did the variation of α_{ion} with anode current. It was previously thought that the fractional number densities of Xe^{+2} and Xe^{+3} only increase as the anode potential is raised. However, after some consideration and further analysis an explanation for this effect became apparent. Discussion of this is presented in the next section.

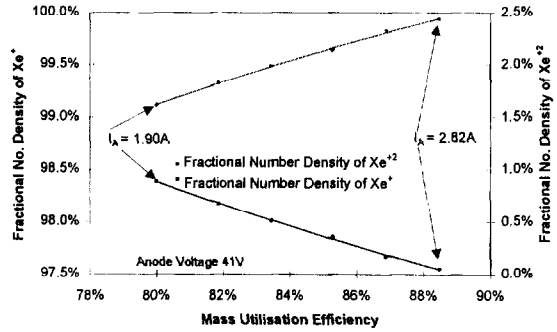

Fig.8 Fractional Number Densities of Xe^{+} and Xe^{+2} vs Anode Current

As stated earlier, the TOFMS can detect singly-charged iron ions and doubly-charged molybdenum ions. The signal levels from these trace elements are much smaller than the xenon ion species and so measuring the ion intensities is subject to sizeable errors.

Table 3 shows a typical set of readings taken for one operating point at all four angular positions. Columns two and three record the heights of the peaks produced by the relevant ions against angular position (shown in column one). Column four shows the relative mass spectral intensities of Xe^{+2} as measured previously. Column five shows the relative mass spectral intensity of Fe^{+} at each angle under investigation. This is simply calculated by dividing the Fe^{+} intensity by the Xe^{+2} intensity and multiplying the result by the relative mass spectral intensity of Xe^{+2}.

Ang. Pos. (deg)	Mass Spectral Intensities		Relative Mass Spectral Intensities (%)		Iron Loss Rate	Composite Iron Loss Rate
	Xe^{+2}	Fe^{+}	Xe^{+2}	Fe^{+}	(g/hour)	(g/hour)
2	2557.4	4.60	8.2	0.0151	4.11E-04	
6	1291.5	4.15	5.4	0.0179	4.88E-04	
10	646.20	2.55	5.5	0.0224	6.12E-04	**5.353E-0**
14	170.07	0.67	6.0	0.0169	4.62E-04	

Table 3
Sample Mass Spectral Intensity Data

The iron loss rate (g/hour) is calculated as follows:

$$Fe_{rate} = Fe_{corr} Fe^{+} I \frac{3600 A_r(Fe)}{N_A e} I_B \quad (3)$$

where:
- Fe_{rate} Rate of loss of iron.
- Fe_{corr} Correction factor.
- $Fe^{+}I$ Relative mass spectral intensity.
- I_B Beam current.
- $A_r(Fe)$ Relative atomic mass of iron.
- N_A Avogadro's number.
- e Charge on an electron.

The correction factor is currently set to a value of four for continuity with earlier work carried out by Aerospace Corporation[1]. This factor attempts to compensate for the contribution of Fe^{+2} ions which cannot be measured and also for the material sputtered and then redeposited in the discharge chamber. It is clearly a major contributor to the substantial experimental errors associated with this analysis, and is examined further in the latter part of this paper.

The composite value of iron mass loss rate is calculated using a similar method to that used to calculate the composite value of α_{ion}.

It would have been advantageous to have measured the Fe^{+} intensities and therefore iron mass loss rates at a constant 18mN for each of the fifteen operating points under investigation. However, to do so would have required a change of main flowrate for each operating point. This would have doubled the time required to carry out these experiments, which the test schedule did not allow.

It was assumed, not unreasonably, that the iron erosion rate is proportional to the ion density for small variations. As the extracted ion current and hence the thrust is proportional to the ion density, it can be said that the iron erosion rate is proportional to the thrust for small thrust variations. During this work the thrust was varied from 82% to 107% of the nominal value i.e. a small variation. Bearing this in mind, it is possible to recalculate the iron erosion rates as if the thruster was operating at 18mN. Fig.9 shows the relationship between anode voltage, anode current and iron mass loss rate normalised to 18mN.

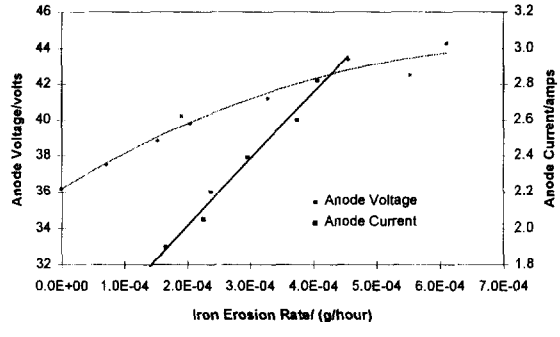

Fig.9 Anode Voltage and Current vs Normalised Iron Erosion Rate

Discussion of Results

Correlation of fractional number densities with ion engine parameters

In the previous section it was shown that the fractional number density of Xe^{+2} and Xe^{+3} present in the beam increase with increasing anode voltage and anode current. The effects of changing anode voltage and current are also seen on α_{ion}, as α_{ion} and the number densities are linked. As the fractional number density of Xe^{+3} was very low and its subsequent effect on α_{ion} is negligible, the contribution from Xe^{+3} will be ignored in the following discussion.

There are two possible causes for the relationship seen between the fractional number density of Xe^{+2} and anode voltage. The first is related to the ionisation cross-sections for the production of Xe^{+} and Xe^{+2}

species which are dependent upon electron energy. The second possible cause is related to the availability of Xe atoms and Xe^+ ions as the mass utilisation efficiency increases.

As the magnetic field strength inside the discharge chamber increases, the average energy required by the electrons to maintain the discharge current at a constant value is increased. This is achieved by raising the anode potential. In effect, increasing the magnetic field strength increases the discharge impedance.

This has two effects which both lead to an increase in mass utilisation efficiency. Firstly, the mean path length of the electrons drawn from the cathode is increased, leading to an improved probability of an encounter with a xenon atom or ion. Secondly, the ionisation cross-sections for the production of Xe^+ and Xe^{+2} increase with increased electron energy up to a limit well beyond the anode potentials used in the T5 ion engine[5]. Note that there are a number of possible ionisation processes for the production of Xe^+ and Xe^{+2} ions, many of them making use of metastable xenon species.

It can be seen from the data that the ionisation cross-sections for the production of Xe^+ are greater than those for the production of Xe^{+2} at typical T5 ion engine anode potentials (35V to 45V). However, if the Xe^{+2} cross-sections increase at a proportionately greater rate than for Xe^+ in the energy range of interest then the fractional number density of Xe^{+2} would be expected to increase at the expense of Xe^+, leading to a reduction in α_{ion}.

The number density of Xe^+ ions present in the discharge chamber is proportional to the product of the number density of xenon atoms and the electron flux density (ignoring the contribution from metastable species and any electron energy variations). If the flowrate of xenon into the discharge chamber is not altered, then an increase in the number density of Xe^+ must be balanced by a reduction in the number density of xenon atoms; the production of Xe^+ becomes more difficult with increasing Xe^+ ion number density. Conversely, as the amount of Xe^+ increases, the production rate of Xe^{+2} increases. Therefore, as the Xe^+ number density increases, the Xe^{+2} number density increases proportionately at a greater rate. In other words, the fractional number density of Xe^{+2} increases with an increase in the mass utilisation efficiency.

A rise in anode current has the effect of increasing the electron flux in the discharge chamber, thereby increasing the number densities of Xe^+ and Xe^{+2}. As the anode potential has not been changed then the average electron energy should remain constant, leading to an unchanged ionisation cross-section.

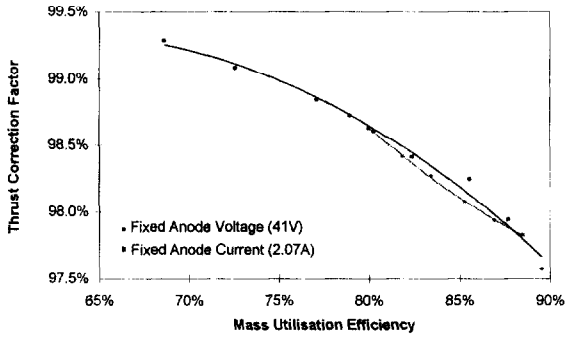

Fig.10 Mass Utilisation Efficiency vs α_{ion}, Fixed Anode Voltage and Fixed Anode Current

If the effects of changing utilisation efficiency on α_{ion} (or fractional number densities) by varying the anode voltage are compared to the effects of varying the anode current it should be possible to determine whether changing ionisation cross-sections or lack of xenon atoms dominate. Fig.10 show plots of mass utilisation efficiency vs α_{ion} for fixed anode voltage (41V) and variable anode current as well as fixed anode current (2.07A) and variable anode voltage. The plots are nearly identical, suggesting that the fractional number density of xenon atoms largely determines the fractional number density of Xe^{+2} and therefore α_{ion} with little contribution, if any, from proportional changes in ionisation cross-sections.

The effect of Xe to Xe^{+2} ionisation cross-section on fractional number densities

The previous sub-section suggests that there is minimal impact on the fractional number density of Xe^{+2} due to proportional changes in ionisation cross-sections as the anode voltage increases. However, it is shown in Reference 5 that the cross-section for the production of Xe^+ is broadly constant from 36eV to 44eV, while the cross-section for the production of Xe^{+2} from Xe atoms increases by a factor of 9 over the same electron energy range. This is not to say that the results from this paper and Reference 5 are contradictory. There are at least three possible reasons why the fractional number density of Xe^{+2} is not driven solely by the anode potential.

Firstly, Reference 5 shows only the ionisation cross-section for the production of Xe^{+2} from atomic xenon. Whereas in the discharge chamber of the ion engine multi-step processes utilising metastable states and Xe^{+} ions may lead to the production of Xe^{+2} ions, all with their associated energy dependent cross-sections. These processes probably account for over half of the Xe^{+2} produced as the energy required at each step in a multi-step process is less than that required in a one step process. Domination by multi-step processes will swamp the single step process and may lead to a very different aggregate cross-section vs electron energy relationship than that presented in Reference 5.

The average energy of the ionising electrons is related but not identical to the anode potential; it is generally assumed to be at least 10eV lower. Also, the electron energies are distributed about the mean value, perhaps in the form of a Poisson distribution. As the ionisation cross-sections vary non-linearly with electron energy, the shape of the distribution will affect the ion production rates for a given average electron energy. Furthermore, the difference between anode potential and average electron energy may vary under the influence of some unkown factor. The impact of such effects is not known.

In the discharge chamber the plasma conditions vary greatly depending upon location (i.e. neutral densities, ion densities, electron flux, electron energies and magnetic flux density). This is in marked contrast to the homogeneous conditions assumed if evaluating the likely ionisation cross-sections and subsequent fractional ion number densities from the anode potential. Furthermore, the discharge plasma is enclosed by the discharge chamber walls which also impact on the ion production rates; much additional work is needed to clarify this issue.

The above mentioned are by no means an exhaustive list of all possible reasons for the fractional number density not to increase with increased anode voltage alone. The impact of the effects mentioned may be negligible or significant.

Iron erosion rate

The iron erosion rate is seen to increase with increasing mass utilisation efficiency as shown in Fig.11. This is to be expected, as the greater the ion density, the higher the rate of collision between ions and the discharge chamber walls and therefore the greater the iron flux from the discharge chamber. There is little difference between the constant anode current case (2.07A) and the constant anode voltage case (41V). What difference there is can be ascribed to experimental error.

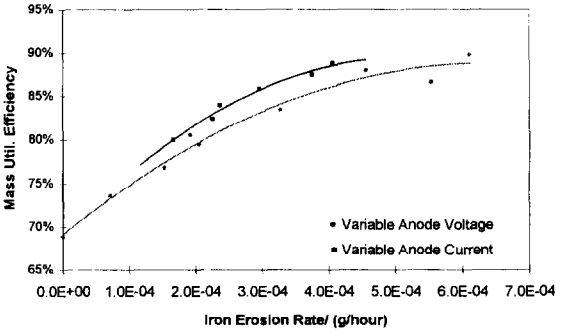

Fig.11 Normalised Iron Loss Rate vs Mass Utilisation Efficiency

Note how the rate of increase of erosion rate increases at the higher mass utilisation efficiencies. This may be attributed to the rise in the proportion of Xe^{+2} to Xe^{+} ions. Naturally, this assumes that a Xe^{+2} ion is more likely to cause sputter damage than an Xe^{+} ion accelerated by the same potential.

Using the iron loss rate data it was possible to estimate the likely discharge chamber life based on work carried out by AEA Culham[2]. Culham showed that a T5 ion thruster would operate satisfactorily despite losing 10g of material from the discharge chamber. A lifetime of 30,000 hours is indicated using the mass loss rate generated at the ARTEMIS[4] operating point.

This estimated lifetime is highly dependent upon the correction factor (Fe_{corr}) of equation (3), used to account for the Fe and Fe^{+2} erosion products not measurable by the TOFMS. Dr. J Pollard had hypothesised[1] that half of the eroded iron would be ionised and extracted and half would be redeposited, assuming that xenon is utilised at 70%-90% and that an iron atom will make a single pass through the plasma and either be ionised or remain neutral and stick to the surface. (This gives a factor of 2 for Fe.). Ionised iron is distributed between Fe^{+} and Fe^{+2}. The latter was seen to contribute somewhat to the 28 amu intensity, so it is present in an amount greater than zero. Crude modelling of the plasma[1] suggested that Fe^{+2} would be dominant at the conditions that could account for the Xe charge state distribution, but then it would be expected for the signal at 28 amu to be more obviously due to Fe^{+2} rather than to the N_2^{+} and CO^{+} background species. It was decided[1] that an iron charge state distribution made up of equal parts Fe^{+}

and Fe^{+2} would be the most plausible assumption. (This gives the factor of 2 for Fe^{+2}.) Combining the factors for Fe and Fe^{+2} gives an overall correction factor of 4.

A similar study was carried out at the Aerospace Corporation using the same facility, TOFMS and ion engine[1]. The ion engine was fitted with engineering model grids and was operated with a beam potential of 1100V rather than 1175V. The plume was analysed at a variety of operating points based on a nominal 18mN of thrust. Greater values for the number densities of Xe^{+2} and Fe^{+} ions were seen, leading to typically lower values for α_{ion} (0.935 to 0.995) and a greater iron loss rate ($8x10^{-4}$ g/hour) at 18mN.

These differences between Reference 1 and this work may be due to the following factors: changes in the TOFMS set-up, a difference in interpreting the raw data, operating with different grid potentials, and the grid set design. Interpretation of the raw data is unlikely to be the sole cause of the sizeable differences seen because the author used the same analysis method as Dr Pollard. The grid potentials, while having an effect on thrust levels and beam divergence have minimal impact on the discharge chamber plasma. The optimised grid design has an effect on the plasma density distribution across the face of the screen grid, which is unlikely to have any impact on the relative intensities of the ion species. However, there were differences in the set-up of the TOFMS. Firstly, the TOFMS used a shortened drift distance for this work, which gave better resolution and sensitivity. Secondly, the time of flight gate widths and multiplier gains were more optimal than used previously. Taking account of both of these operational improvements, Dr. Pollard believes that the newer data are more accurate. Although it seems unlikely that the grid potential or grid design would have a significant impact on the relative ion intensities, such possible effects cannot be discounted.

Conclusions

The TOFMS is well suited to determining the doubly and triply-charged ion content of the beam. The resolution of the data was more than adequate for determining values of α_{ion} to an acceptable accuracy. However, the ratio of Xe^{+2} to Xe^{+} seems to be a function of the mass utilisation efficiency rather than the anode potential as thought previously. This is an important finding and was completely unexpected, although a satisfactory explanation for it has been found.

The intensity of Fe^{+} at all operating conditions and especially at the larger angles was very low, which introduced sizeable errors. Despite this, sensible mass loss rates were developed which increased with increasing mass utilisation efficiency.

The derived lifetime compares well with that observed in lifetests carried out by other groups. As an example, several MELCO thrusters were operated in parallel for in excess of 10,000 hours, passing the qualification requirements for flight[6].

The best method for determining the lifetime of an ion thruster is to set up a lifetest. The work carried out with the TOFMS and other work involving grid-set erosion can be used to identify an optimum operating point for a prospective lifetest programme, avoiding the scenario where the operating conditions need to be changed part way through a lifetest. Such studies can also clarify the lifetime implications of design changes more quickly than is possible by long-duration testing.

Acknowledgements

Most of the results used here were generated as part of work funded by Matra Marconi Space to improve the understanding of how the T5 ion thruster performs around the 18mN operating point chosen for ESA's ARTEMIS communications satellite programme. The author would like to thank The Aerospace Corporation and in particular Dr. Jim Pollard for operating the time of flight mass spectrometer and advising on the data analysis.

References

1. Pollard, J E, *'Plume Angular, Energy, and Mass Spectral Measurements with the T5 Ion Engine'*, AIAA, Paper 95-2920 (July 1995).
2. Hurford, P, *'UK-10 Ion Thruster 3 Grid, 500 Hour Lifetest'*, LP-63104-TNO-0043, AEA Technology, (January 1993).
3. Fearn, D G, Martin, A R, Smith, P, *'Ion propulsion development in the UK'*, IAF, Paper 93-S.5.490, (June 1993).
4. Renault, H, Silvi, M, Bohnhoff, K, Gray, H, *'Electric propulsion on ARTEMIS a development status'*, Proc. 2nd European Spacecraft Propulsion Conference, ESTEC, Noordwjik, ESA SP-398, (1997)
5. Syage, J A, *'Electron impact cross sections for multiple ionisation of Kr and Xe'*, Phys. Rev. A, vol. 46 p. 5666, (1992).
6. Shimada, S, Satoh, K, Gotoh, Y, Nishida, E, Noro, T, Takegahara, H, Nakamaru, K, Nagano, H, 'Ion thruster endurance test using development model thruster for ETS-VI', IEPC Paper 93-169, (September 1993).